Geophys. Astrophys. Fluid Dynamics, Vol. 51, pp. 35–52
Reprints available directly from the publisher
Photocopying permitted by license only

SOLITARY WAVES ON CONDUITS OF BUOYANT FLUID IN A MORE VISCOUS FLUID*

KARL R. HELFRICH and JOHN A. WHITEHEAD

Woods Hole Oceanographic Institution, Woods Hole, MA 02543, USA

(*Received 29 March 1989; in final form 23 May 1989*)

Fluid of a lower density and viscosity can buoyantly rise through a viscous fluid through conduits that support simple pipe flows. The conduits also support solitary waves which exhibit near soliton behavior. Laboratory experiments on the characteristics of the solitary waves and their interactions have been conducted and compared with theory. The observations of shape and phase speed of individual waves show good agreement with the theoretical predictions. Large amplitude waves traveled slightly faster than the theoretical predictions. The discrepancy is probably due to higher order effects associated with wave slope not accounted for in the theory. Individual wave characteristics (shape, amplitude and speed) were very nearly preserved after collision with another wave. A phase jump of each wave was the main consequence of an interaction. The larger (faster) waves increased in amplitude by an average of 5 percent after collision and their phase speeds decreased by an average of 4 percent. The small wave was unchanged. Numerical solutions overpredicted the magnitude of the observed phase jumps by about 40 percent when compared to the experiments.

It is also shown theoretically and confirmed experimentally that the solitary waves have closed streamlines in a frame moving with the wave. Thus, transport of isolated packets of fluid over large distances will occur. Wave interactions result in the transfer of trapped fluid between the interacting waves.

KEY WORDS: Solitary waves, solitons, convective plumes, mantle convection.

1. INTRODUCTION

A steady source of an intrusive buoyant low viscosity fluid at the bottom of a more viscous external fluid will result in the development of a uniform conduit which supports simple pipe (Poiseuille) flow if the Reynolds number is small (Whitehead and Luther, 1975). The buoyancy of the intrusive fluid is balanced by shear stress. When the source is unsteady it has been shown that the conduits support solitary waves (Scott *et al.*, 1986; Olson and Christensen, 1986). It has also been noted that interaction of solitary waves results in soliton-like behavior. Both these studies utilized both theory and experiments; however, the only quantitative comparison made was of the wave dispersion relation (Olson and Christensen, 1986). Somewhat more extensive measurements were made by Whitehead (1987) who reported that wave amplitudes were conserved to better than ten percent upon collision. It is the purpose of this paper to make a more complete comparison of laboratory experiments with the theoretical description of solitary waves and their interactions on conduits. Furthermore, we demonstrate theoreti-

*Woods Hole Oceanographic Institution Contribution No. 6848.

cally and experimentally that the solitary waves convey isolated pockets of conduit material with them as they propagate.

Interest in the conduits is severalfold. The first is that these conduits are yet another system in which solitary waves and soliton-like behavior are robust features. From the perspective of geology and geophysics the conduits are a simple analog of one-dimensional compaction driven flow in a porous viscous matrix (Scott *et al.*, 1986). The conduit area is analogous to the porosity of the matrix, the intrusive fluid to the buoyant interstitial melt and the exterior fluid to the deformable crystalline matrix which makes up the mantle. For specific conditions relating the bulk viscosity and permeability of the matrix to the porosity, the conduit equations (see (2.6) and (2.7) below) are equivalent to the equations describing compaction driven flow. The compaction flow equations also have solitary wave solutions termed "magmons" (Richter and McKenzie, 1984; Scott and Stevenson, 1984). Compaction driven flows are relevant to problems of melt migration in the mantle such as formation of melt under mid-ocean spreading centers.

The dynamics of the conduits are also of interest because such structures may exist in the earth as a result of thermal convection plumes from the core–mantle boundary (Morgan, 1971; Olson *et al.*, 1987). Conduits would convey large amounts of material from deep in the earth to the surface quickly and continuously. They may be associated with hot spots and the formation of volcanic island chains.

Another reason for this study is that these waves can apparently persist as solitary waves with near soliton behavior up to very large amplitudes. One purpose here is to determine if the theory is applicable for large waves, even though the assumption of a small slope is used to arrive at the wave equations.

The paper is organized as follows. The theoretical background and mass transport properties of solitary waves are given in Section 2. Section 3 describes the experimental set-up. The results are discussed in Section 4, and Section 5 contains a summary.

2. THEORETICAL BACKGROUND

Consider the situation in which a conduit of buoyant low viscosity fluid rises vertically through a more viscous exterior fluid. If the viscosity of the external fluid is much greater than the intrusive fluid, steady flow in the conduit is of the Poiseuille type (Whitehead and Luther, 1975). The buoyancy of the intrusive fluid provides the driving force which is balanced by shear stress. If the conduit mass source is unsteady waves will develop on the conduit. These waves are governed by (Scott *et al.*, 1986; Olson and Christensen, 1986):

$$\frac{\partial A'}{\partial t'} + \frac{\partial Q'}{\partial z'} = 0, \tag{2.1}$$

$$Q' = -\frac{A'^2}{8\pi\mu_i}\frac{\partial P'}{\partial z'}, \tag{2.2}$$

$$P' = -(\rho_e - \rho_i)gz' + \frac{\mu_e}{A'}\frac{\partial A'}{\partial t'}, \tag{2.3}$$

where A' is the cross-sectional area of the conduit, Q' is the volumetric flux in the conduit, P' is the pressure deviation in the conduit from hydrostatic pressure, g is the acceleration due to the gravity, ρ is the density, μ is the dynamic viscosity, z' is the vertical coordinate and t' is the time. The subscripts i and e refer to the intrusive and exterior fluids respectively and the primes are used to denote dimensional variables. Equation (2.1) is a statement of continuity and (2.2) is the Poiseuille flow relation which is valid locally provided the wave slope is small. The relationship for pressure within the conduit (2.3) consists of a buoyancy induced term and a contribution due to temporal variations in the conduit area. This last term arises because variations in conduit size induce flow in the exterior fluid. The small wave slope assumption is necessary to arrive at this general form.

It is convenient to normalize (2.1)–(2.3) with

$$A = A'/A_0, \qquad z = z'/L, \tag{2.4}$$

$$Q = Q'/Q_0, \qquad t = t'/T.$$

The lengthscale L and the timescale T are given by

$$L = \left(\frac{\mu_e A_0}{8\pi\mu_i}\right)^{1/2}, \tag{2.5a}$$

$$T = \frac{1}{g(\rho_e - \rho_i)}\left(\frac{8\pi\mu_i\mu_e}{A_0}\right)^{1/2}, \tag{2.5b}$$

and a velocity scale U is defined as

$$U = L/T = Q_0/A_0. \tag{2.5c}$$

Here A_0 and Q_0 are the area and flowrate of the undisturbed conduit. Equations (2.1)–(2.3) become, after eliminating P' and using (2.1) to eliminate $\partial A'/\partial t'$ in (2.3),

$$\frac{\partial A}{\partial t} + \frac{\partial Q}{\partial z} = 0, \tag{2.6}$$

$$Q = A^2\left[1 + \frac{\partial}{\partial z}\left(\frac{1}{A}\frac{\partial Q}{\partial z}\right)\right]. \tag{2.7}$$

It can be shown that (2.6) and (2.7) reduce to the Korteweg–de Vries (KdV) equation in the limit of small wave amplitudes (Whitehead and Helfrich, 1986). However, the range of validity of the KdV equation is very limited. The experiments described below were designed to test (2.6) and (2.7) well beyond the small amplitude range.

Solitary wave solutions to (2.6) and (2.7) are given by (Olson and Christensen, 1986):

$$\frac{dA}{d\xi} = \pm \frac{A}{c^{1/2}} (1 + c - 2cA^{-1} - 2 \ln A - (1-c)A^{-2})^{1/2}, \tag{2.8}$$

where $A = A(\xi)$ and $\xi = z - ct$. Here c is the nondimensional phase speed of the wave (normalized by U) which is related to the wave amplitude or maximum area $A_m = A(0)$ through the dispersion relation

$$c = (2A_m^2 \ln A_m - A_m^2 + 1)/(A_m - 1)^2. \tag{2.9}$$

In the limit $A_m \to 1$ we have $c \to c_0 = 2$, the linear long wave phase speed. This velocity is equal to the maximum (centreline) fluid velocity in an undisturbed conduit (see (2.11) below). For $A_m \gg 1$, (2.8) can be integrated to give (Olson and Christensen, 1986):

$$A(\xi) = A_m e^{-\xi^2/2c}.$$

Solutions to (2.6) and (2.7) representing nonlinear wavetrains also exist (Olson and Christensen, 1986) but will not be studied here. The dispersion relation (2.9) and the wave solutions found by numerical integration of (2.8) are compared with experiments in Section 4.

Early numerical solutions of the compaction equations (Scott and Stevenson, 1984; Richter and McKenzie, 1985) implied that collisions between two solitary waves were conservative, a phase shift of each wave being the only product, therefore waves appeared to exhibit soliton properties. However, Barcilon and Richter (1986) demonstrated that the one-dimensional compaction equations do not have exact soliton properties. Their high resolution numerical experiments showed that collisions produced a weak dispersive tail. The amplitude of the tail and the mass and energy contained in it were less than $O(10^{-2})$ compared with the original waves. The waves were very slightly altered during the collision, yet the only significant effect was a phase shift of each wave. However, for practical purposes, the numerical solutions showed that wave interaction results only in phase shifts.

Another important feature is the conveyance of mass by the waves. The details of the flow field within the conduit induced by a solitary wave can be theoretically determined. First the velocity profile within the conduit will be found. From the assumption of Poiseuille flow, the velocity profile is (in dimensional form),

$$u'(r', z', t') = \frac{-1}{4\mu_i} (a'^2 - r'^2) \frac{\partial P'}{\partial z'}. \tag{2.10}$$

Here $a' = (A'/\pi)^{1/2}$ is the radius of the conduit and r' is the radial coordinate. Using (2.3) to eliminate P' and nondimensionalizing (2.10) with (2.5) we have

$$u = 2A\left(1 - \frac{r^2}{A}\right)\left[1 + \frac{\partial}{\partial z}\left(\frac{1}{A}\frac{\partial Q}{\partial z}\right)\right]. \tag{2.11}$$

Here r' has been nondimensionalized with the base conduit radius $(A_0/\pi)^{1/2}$. Equation (2.11) is valid for $0 \leqq r \leqq A^{1/2}$.

If we consider a solitary wave given by the solution of (2.8), then (2.6) gives

$$\frac{dQ}{d\xi} = c\frac{dA}{d\xi}.$$

After integrating and recalling that $Q=1$ when $A=1$ we have

$$Q = cA + 1 - c.$$

Using this in (2.7) we get

$$\left[1 + \frac{\partial}{\partial z}\left(\frac{1}{A}\frac{\partial Q}{\partial z}\right)\right] = (cA + 1 - c)A^{-2},$$

which can be used to reduce (2.11) to

$$u = 2\left(1 - \frac{r^2}{A}\right)(cA + 1 - c)A^{-1}. \tag{2.12}$$

The maximum velocity u_m within the conduit is located at $(r, \xi) = (0, 0)$. Since $A = A_m$ at $\xi = 0$ (2.12) gives

$$u_m = 2A_m^{-1}(cA_m + 1 - c). \tag{2.13}$$

It can be shown using (2.9) and (2.13) that $u_m/c > 1$ for all $A_m > 1$. Fluid in the wave is moving faster than the wave and stagnation points must exist along the axis $r=0$ both ahead of and behind $\xi = 0$ (in a reference frame moving with the wave). Recall that ahead and behind the wave $A=1$ and $u=2$, which is less than u_m. This shows that *all* solitary waves contain trapped fluid.

The region of trapped fluid is defined by closed streamlines in a reference frame moving with the wave phase speed. Defining the streamfunction ψ such that

$$v = -\frac{1}{r}\frac{\partial \psi}{\partial \xi}, \qquad u' = \frac{1}{r}\frac{\partial \psi}{\partial r},$$

where v is the radial velocity and $u' = u - c$ is the vertical velocity in the moving reference frame we have

$$\psi - \psi_0 = \int r(u'dr - vd\xi). \tag{2.14}$$

If the line integral is taken in a plane $\xi = \text{constant}$, (2.12) and (2.14) give

$$\psi(r,\xi)-\psi_0=\left(\frac{cA+1-c}{A}\right)\left(r^2-\frac{r^4}{2A}\right)-\frac{cr^2}{2}. \tag{2.15}$$

Here ψ_0 is the value of the ψ at the axis $r=0$, which is constant since $\partial\psi/\partial\xi=0$ at $r=0$.

Since (2.15) is a measure of the mass flux between the centreline and some radius r, the location r^* where (2.15) is equal to zero defines the streamline enclosing the trapped fluid

$$r^*=\left[2A-c\left(\frac{A^2}{cA+1-c}\right)\right]^{1/2},$$

as a function of ξ through the solitary wave solution $A(\xi)$. The stagnation points occur where $r^*=0$. Figure 1(a) shows the streamlines for an example with $A_m=10$. Also shown in Figure 1(b) is the profile of vertical velocity at $\xi=0$ relative to the moving reference frame. The trapped fluid circulates by ascending in the center and descending at some larger radius. Figure 2 shows the ratio of the volume of trapped fluid (determined numerically from (2.15)) to the volume anomaly of the wave as a function of the wave amplitude A_m. The volume of trapped fluid is less than, but the same order of magnitude as, the volume anomaly of the wave. The ratio quickly approaches one as the amplitude increases.

2.1 Numerical Methods

In the discussion of experimental results in Section 4 use is made of numerical solutions of the conduit equations (2.6) and (2.7). The numerical method follows Barcilon and Richter (1986). The areas $A_j^m=A(j\Delta z, m\Delta t)$ and fluxes $Q_{j-1/2}^m$ are defined on staggered grids. Here Δz and Δt are the space and time steps respectively. From the areas at some time $t=m\Delta t$ the corresponding flux distribution is found from (2.7). Employing second-order finite-differences this gives

$$(1-b_{j+1/2})Q_{j+3/2}^m-2\left(1+\frac{(\Delta z)^2}{A_{j+1/2}}\right)Q_{j+1/2}^m+(1+b_{j+1/2})Q_{j-1/2}^m=-A_{j+1/2}(\Delta z)^2, \tag{2.16}$$

where

$$b_{j+1/2}=\tfrac{1}{4}\ln\left(\frac{A_{j+3/2}^m}{A_{j-1/2}^m}\right),$$

$$A_{j+1/2}=(A_{j+1}+A_j)/2.$$

Provided the disturbances are kept far from the boundaries, the relation $Q_{1/2}=Q_{N+1/2}=1$ holds. Equation (2.16) then results in a matrix equation of tridiagonal form which is solved by standard methods. An estimate for the area at $t=(m+1/2)\Delta t$ is found from (2.6) as

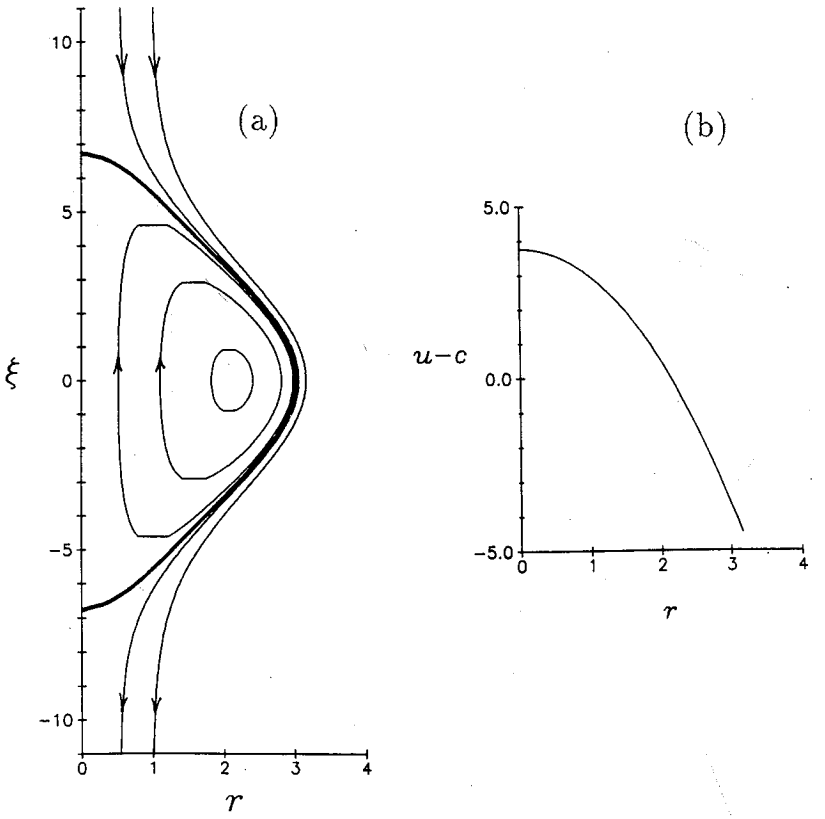

Figure 1 (a) Streamlines in a reference frame moving with the phase speed for a solitary wave with $A_m = 10$. The thick solid line encloses the trapped fluid. (b) Profile of vertical velocity at $\xi = 0$ in the reference frame moving with the wave.

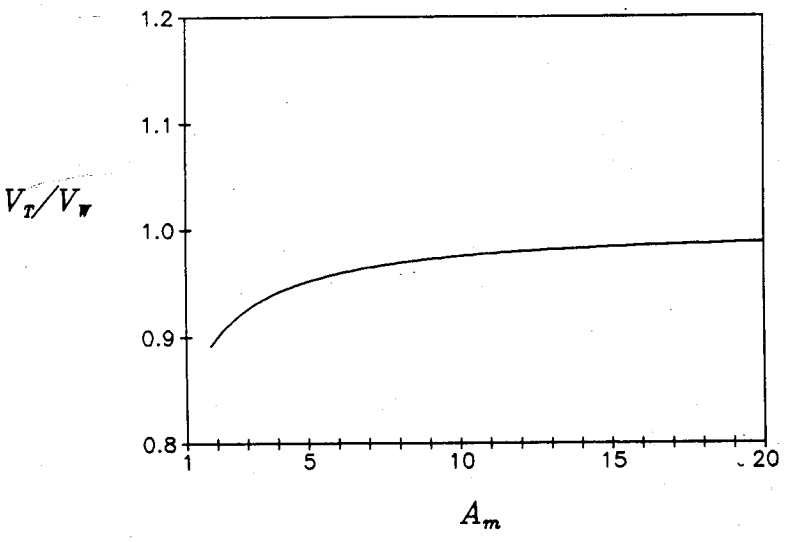

Figure 2 Ratio of the volume of trapped fluid to the volume anomaly as a function of A_m.

$$A_j^{m+1/2} = A_j^m - \frac{\Delta t}{2\Delta z}(Q^m_{j+1/2} - Q^m_{j-1/2}).$$

Then (2.16) is solved for $Q^{m+1/2}_{j+1/2}$ and the areas at $t=(m+1)\Delta t$ are found from

$$A_j^{m+1} = A_j^m - \frac{\Delta t}{\Delta z}(Q^{m+1/2}_{j+1/2} - Q^{m+1/2}_{j-1/2}).$$

The method was checked by allowing solitary wave solutions of (2.8) to propagate over approximately 50 wave length scales. The mass of the waves were conserved to within one percent and the computed phase speeds agreed with (2.9) to within the same accuracy. The space and time steps used in the numerical integrations were $\Delta z = 0.3$ and $\Delta t = 0.05$.

Phase shifts from numerical calculations of solitary wave interactions were evaluated for comparison with the experimental results. To improve the accuracy of the phase shift estimates the location of a wave crest after collision (usually between grid points) was found by fitting a cubic spline to the five grid points closest to the wave crest. The maximum value of the interpolating polynomial was identified as the crest.

3. EXPERIMENTAL METHOD

The experiments were conducted in a glass tank 10 cm by 10 cm in cross section and 120 cm deep. The tank was filled approximately 110 cm deep with Karo corn syrup. The intrusive fluid, a 70:30 mixture by volume of Karo syrup and water dyed blue for visualization, was introduced through a hollow tube positioned over the centre of the tank bottom. Previous experiments (Whitehead, 1987) have been hindered by a conduit which was a few degrees out of vertical. To generate a straight conduit, the tube was connected to an air supply and bubbles were slowly bled in. The tube was then switched to a reservoir of intrusive fluid. The final rising air bubbles caused the intrusive fluid to rise vertically in their wake, leaving a straight vertical conduit.

The reservoir was positioned so that the free surface was 13 cm above the free surface level in the tank. This constant pressure generated a conduit whose diameter remained steady for all the experiments. A solitary wave was generated by raising the reservoir level a specified height for a fixed time then returning it to the base level. This method resulted in the generation of clean individual solitary waves. Photographs of waves were taken with a 35 mm camera mounted on a vertical shaft which allowed the camera to be manually moved in order to follow the trajectory of the waves. The camera was positioned 1 m away from the conduit, and the use of a telephoto lens enabled close up photographs against an opaque background on the rear face of the tank which included a scale. Parallax errors and errors due to refractive index variations around the conduit were estimated to be less than 2 percent.

Runs commenced by generating a "slow" small amplitude wave. After a given time interval a second "fast" large amplitude wave was produced. Photographs were taken automatically at timed intervals of either two or three seconds. Data were obtained by projecting slides onto a screen and measuring wave amplitudes,

Table 1 Physical and scaling quantities

Fluid		$\rho(gm\,cm^{-3})$	$\mu(gm\,cm^{-1}\,s^{-1})$
external (Karo syrup)		1.424	45.0 ±4.5
intrusive (70:30 syrup and water mixture by volume)		1.257	0.40±0.04
A_0	L	T	$U=L/T$
0.0115 cm^2	0.23 cm	1.24 s	0.185 cm s^{-1}

shapes and positions (denoted by the location of the maximum amplitude). The wave locations could be measured to within 0.1 cm and the conduit and wave diameters to within 0.005 cm.

The major sources of uncertainty in the experiments were the viscosities of the external and intrusive fluids. Densities were measured using a precision balance and densimetric flask. The viscosity of the external fluid was estimated by timing the fall of steel spheres through the fluid and then applying Stokes' relation. Numerous trials with several different diameter spheres gave a consistent average of $\mu_e = 45.0\,\mathrm{gm\,cm^{-1}\,s^{-1}}$. The viscosity of the intrusive mixture was determined using a standard glass Poiseuille-type viscometer to be $\mu_i = 0.40\,\mathrm{gm\,cm^{-1}\,s^{-1}}$. In both determinations care was taken to have the temperatures of the fluids equal to $23 \pm 1\,^{\circ}\mathrm{C}$, the temperature in the experimental apparatus. The viscosity estimates are good to within ±10 percent.

The physical characteristics of the fluids, the base conduit area A_0, and the scaling quantities L, T and $U = L/T$ are summarized in Table 1. The values shown for A_0, L, T and U were used to nondimensionalize the results presented in the next section.

4. DISCUSSION OF RESULTS

A photo montage of a typical collision event is shown in Figure 3. The individual waves both before and after the collision are isolated. Detection of a weak dispersive tail generated by the collision was unsuccessful and was concluded to be beyond the sensitivity of these experiments. A phase shift of each wave was easily observed. The summary of wave characteristics and results from 10 experimental runs in which 11 collision events occurred is given in Table 2.

4.1 Individual Waves

Before discussing the collision events we first examine the characteristics of individual waves away from the interaction region. In Figure 4 the measured phase speeds are plotted as a function of amplitude A_m for all the experiments. Phase speeds were determined by a linear least squares fit of position vs. time using data away from the interaction region (see Figure 7). The computed slopes had correlation coefficients of 0.999 or better. The figure contains data for both

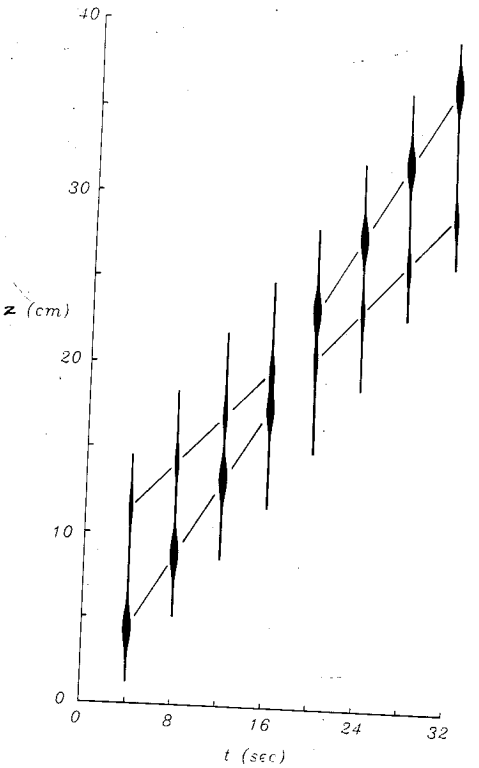

Figure 3 Photomontage of a collision event (run 3)

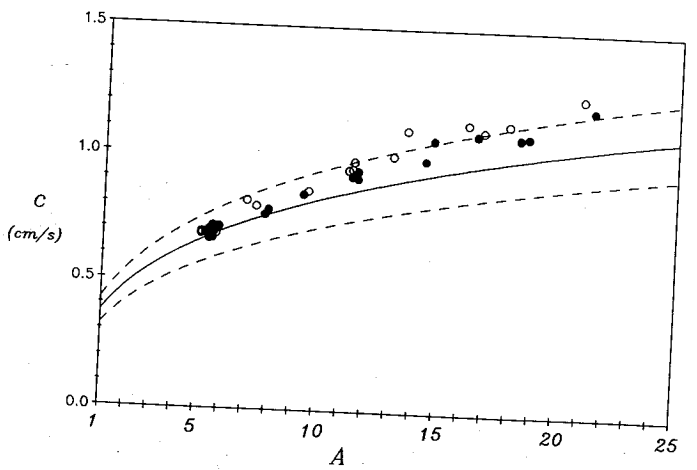

Figure 4 Measured phase speeds (dimensional) as a function of nondimensional wave amplitude; ○, before collision; ●, after collision. The solid line is the theoretical dispersion relation (2.9) corresponding to the measured fluid properties ($c_0 = 0.37\,\mathrm{cm\,s^{-1}}$). The dashed lines are for $c_0 = 0.32$ and $0.42\,\mathrm{cm\,s^{-1}}$ which correspond to the uncertainty in the fluid properties.

Table 2 Summary of the quantitative measurements from the laboratory experiments. Shown are the maximum areas of waves before (A_i) and after (A_f) the collision normalized by A_0, phase speeds before and after the collision normalized by U, ratios of amplitudes and phase speeds, and the phase jumps normalized by L. In column 1, S denotes the small slow wave and F the large fast wave

Run	A_i	±	A_f	±	A_i/A_f	c_i	c_f	c_i/c_f	Δz
3*S*	5.12	0.09	5.43	0.05	0.94	3.74	3.78	0.989	−8.30
3*F*	16.13	0.13	16.53	0.33	0.98	6.14	5.90	1.045	6.31
4*S*1	5.12	0.11	5.43	0.12	0.94	3.70	3.73	0.991	−8.46
4*F*1	20.96	0.08	21.42	0.31	0.98	6.73	6.49	1.037	5.35
4*S*2	5.43	0.12	5.27	0.15	1.03	3.73	3.73	1.000	−8.86
4*F*2	11.36	0.28	11.36	0.28	1.00	5.13	4.97	1.032	7.26
5*S*	5.59	0.08	5.59	0.16	1.00	3.87	3.89	1.007	−8.60
5*F*	13.59	0.13	14.71	0.13	0.92	1.106	1.069	1.035	5.91
6*S*	5.78	0.16	5.59	0.16	1.03	3.85	3.74	1.029	−8.26
6*F*	11.42	0.28	11.59	0.17	0.99	5.29	5.09	1.039	5.95
7*S*	5.59	0.35	5.47	0.08	1.02	3.76	3.59	1.045	−8.15
7*F*	7.39	0.27	7.76	0.14	0.95	4.31	4.14	1.042	7.80
8*S*	5.59	0.19	5.59	0.16	1.00	3.76	3.77	1.025	−7.95
8*F*	6.99	0.22	7.90	0.14	0.88	4.42	4.24	1.043	9.51
9*S*	5.55	0.16	5.43	0.12	1.02	3.71	3.61	1.031	−6.59
9*F*	11.20	0.11	11.59	0.17	0.97	5.11	4.94	1.036	7.80
10*S*	9.55	0.12	9.35	0.14	1.02	4.65	4.57	1.017	−9.60
10*F*	13.04	0.22	14.39	0.17	0.91	5.43	5.35	1.015	8.95
11*S*	5.74	0.09	5.86	0.07	0.98	3.71	3.85	0.962	−8.40
11*F*	16.80	0.11	18.33	0.21	0.93	5.99	5.86	1.106	6.66
12*S*	5.62	0.08	5.60	0.15	1.00	3.72	3.72	1.000	−8.36
12*F*	17.85	0.09	18.68	0.20	0.96	6.14	5.89	1.042	6.66
Average	Slow				1.00			1.01	
	Fast				0.95			1.04	

before and after the interactions. Also shown are the theoretical dispersion relationship (2.9) and estimated errors based upon uncertainty in the fluid properties. For $A_m \lesssim 10$ the theory and experiment agree quite well. For $A_m \gtrsim 10$ the measured phase speeds are generally larger than the theoretical predictions.

A likely explanation for this difference is that the small slope assumption required for the Poiseuille flow relation (2.2) and used to determine the external fluid contribution to the conduit pressure (2.3) has been violated. The parameter assumed to be small in deriving the correction to the conduit pressure due to the presence of waves is $ka \sim 2\pi(a_m - a_0)/\lambda$, where a_m is the maximum radius of the wave, a_0 is the base conduit radius and λ is a measure of the wave length (half width of a solitary wave). From the experiment $ka \approx 0.1$ for $A_m \approx 5$ and $ka \approx 0.25$ for $A_m \approx 10$. The Poiseuille flow assumption is valid for slowly varying conduits provided (Batchelor, 1967) $\alpha a u \rho_i/\mu_i \ll 1$, where α ($\approx ka/2\pi$) is the conduit wall slope and u ($\approx c$) is a representative conduit flow velocity. This gives the relative importance of inertial to viscous effects. For the experimental parameters and $A_m = 10$ we have $u \approx 2\,\mathrm{cm\,s^{-1}}$, $a \approx 0.6\,\mathrm{cm}$, $ka \approx 0.25$ and $\mu_i/\rho_i = 0.32\,\mathrm{cm^2\,s^{-1}}$. This gives $\alpha a u \rho_i/\mu_i \approx 0.15$. The assumptions on conduit slope and Poiseuille flow are starting to be violated. Furthermore, we must have $ka \ll 1$ for the presence of the tank walls not to be important in the derivation of (2.3).

In a similar set of experiments, Olson and Christensen (1986) also found that

larger waves traveled faster than the theoretical prediction. When their results (plotted as phase speed vs. disturbance volume), are converted to speed vs. amplitude using the solitary wave solution (2.8) we find that waves with $A_m \gtrsim 13$ move faster than predicted. Their results are consistent with the present study. They also attributed the error to large wave slopes.

In Figure 5 measured wave shapes are compared with the solitary wave profiles found from numerical solution of (2.8). The measured amplitudes were used in the calculations. The experimental data for each case came from a photograph prior to the interaction. The numerically and experimentally determined shapes agree quite well over the range of amplitudes realized in the experiments. Even at $A_m = 20.96$ the agreement is good despite the error in the theoretical dispersion relation. Comparisons with wave shapes after the collisions gave equally good results.

Experimental evidence for the presence of trapped fluid is shown in Figure 6. The figure is a time sequence of photographs which show the circulation of dyed flluid within a solitary wave made in a clear conduit. To produce this picture the experimental apparatus was altered so that a second intrusive fluid inlet tube was positioned at an oblique angle to the conduit and slightly above the first inlet. The second tube was connected to a reservoir of dyed intrusive fluid. The wave was produced by elevating both reservoirs, causing some dyed fluid to be introduced into the wave. From Figure 6 it is clear that the dyed fluid is trapped within the wave and propagates with the wave phase speed as it circulates within the centre of the wave: ascending along the centreline and descending at some larger radius. The photographs are qualitatively similar to the streamline pattern shown earlier in Figure 1(a). Trapping of fluid is an observable feature of all the experiments.

4.2 Wave Interactions

In Figure 7 two phase diagrams (z vs. t) are shown. The phase speeds of the waves away from the interaction regions are constant as discussed above. Figure 7(a) shows an experiment in which three waves were present. The first, and smallest, wave interacted twice. The difference in amplitudes, and therefore phase speeds, are relatively large. The interactions occurred quickly over a length of about one to two wave lengths. In Figure 7(b) the two waves are nearly the same amplitude and the interaction takes much longer, about five wave lengths. In all experiments the only obvious effect of the interaction is phase shifts.

Further information regarding the effects of interactions is given in Table 2 where wave amplitudes and phase speeds, before and after the collisions, and phase shifts are tabulated. There was an average increase of the amplitude (maximum area) of the larger wave by about five percent. On average the amplitude of the smaller wave did not change. Scott *et al.*, (1986) state that their experiments showed a tendency for the large wave to increase slightly at the expense of the small wave. The phase speed of the small wave did not change significantly upon interaction; however, the speed of the large wave decreased by an average of four percent. These results can be seen clearly in Figure 4 where the solid symbols representing post-interaction are shifted slightly to the right and down for the larger waves. The post-interaction phase speed data disagree with (2.9) in one sense since an increase in amplitude should correspond to an increase in phase speed yet they give a slightly better agreement with the theoretical curve.

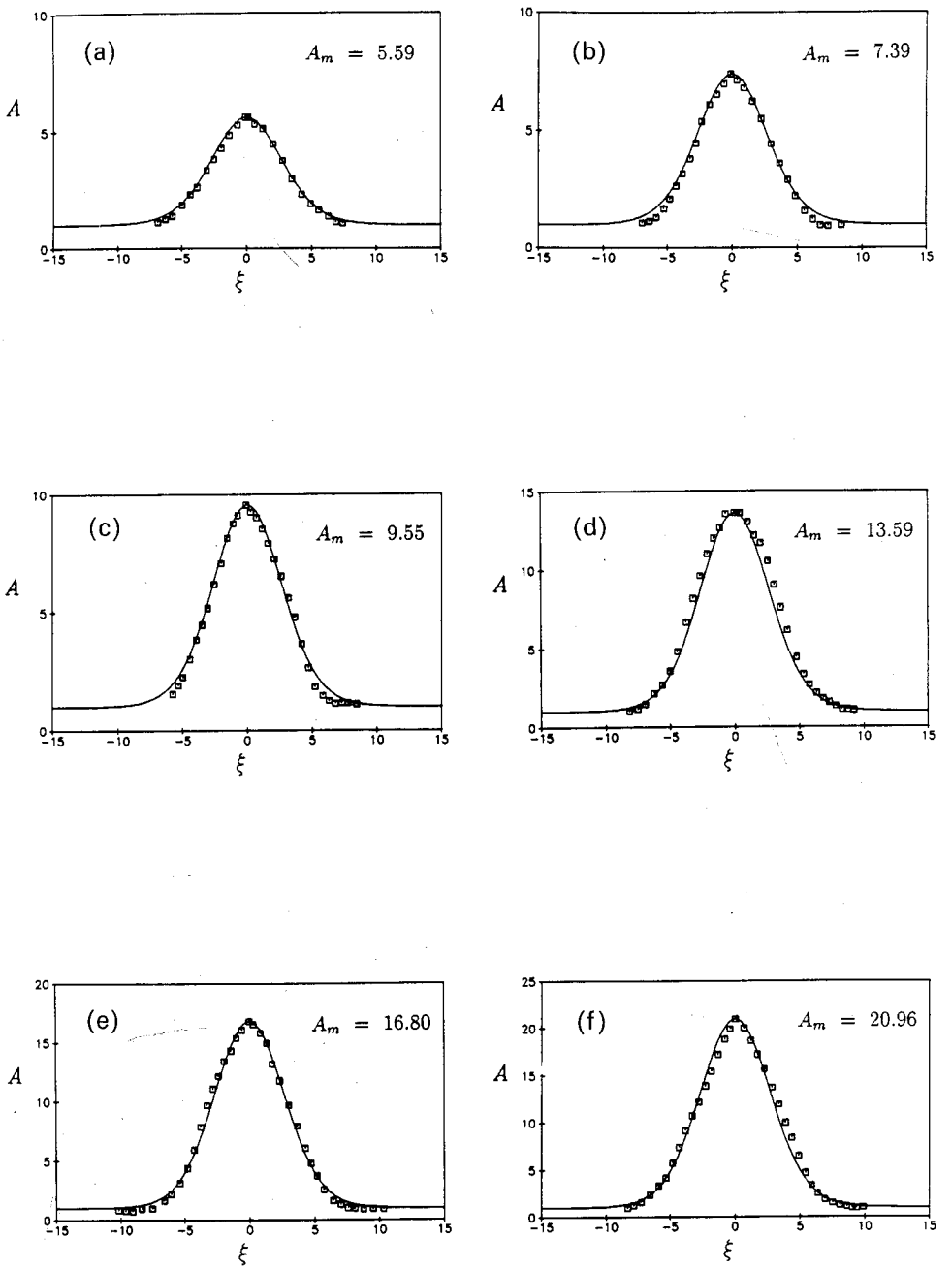

Figure 5 Comparison of measured solitary wave profiles (□) with the theoretical solution (———) numerically calculated from (2.8) for A_m=(a) 5.59, (b) 7.39, (c) 9.55, (d) 13.59, (e) 16.80, (f) 20.96.

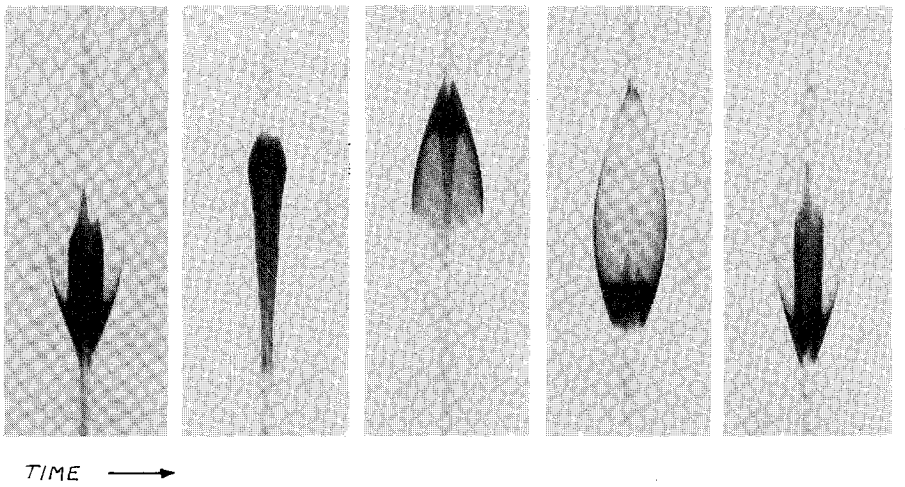

Figure 6 Time sequence of photographs at about 1 s intervals showing circulation of dyed fluid in a solitary wave in a clear conduit.

For a hypothetical collision event between two waves with initial amplitudes of 5.0 and 15.0 (typical of the experiments) a five percent increase in the amplitude of the large wave requires a 15 percent decrease in the amplitude of the small wave if transported mass is to be conserved between the two waves. This calculation was made using the theoretical wave shapes (2.8) and trapped mass region (2.15). A 15 percent decrease in the small wave amplitude is much larger than either the measured amplitude changes of the errors in measured amplitudes shown in Table 2. The cause for the amplitude increase of the large wave is not understood. It could be that interaction entrains some conduit fluid into the trapped region, but there is no clear experimental evidence for any entrainment.

A further comparison of the theory and experiments is shown in Figure 8, where numerically calculated phase shifts are plotted against the experimental measurements. The numerical calculations used the measured wave amplitudes from an experimental run (prior to the interactions) and the corresponding solitary wave solutions from (2.8) as the initial conditions. The experimental phase shift data were determined from offsets at the center of the interaction region in the linear fits to the position data from before and after the interaction. The numerical solution to the conduit equations overpredict the magnitude of the phase shift by about 40 percent for both the large and small waves. The reason for the disagreement is unclear, but again may have to do with the violation of the small slope or Poiseuille flow assumptions.

The transfer of trapped fluid between interacting waves is shown in Figure 9. A large wave containing a trapped parcel of dyed fluid is initially behind a small clear wave on a clear conduit (undyed fluid). When the large wave catches the small wave it injects some dyed fluid into the lead wave. The lead wave is then enlarged and propagates away from the diminished trailing wave. This exchange of identities (amplitudes) is a common feature of solitary wave interactions in many physical systems. However, in this situation the new lead wave now contains trapped fluid particles from both of the interacting waves. The trailing wave contains only fluid from the original trailing wave.

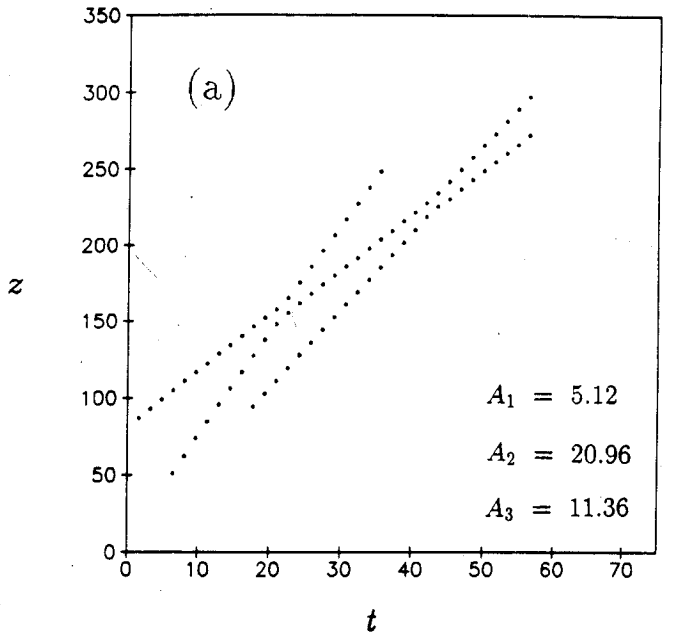

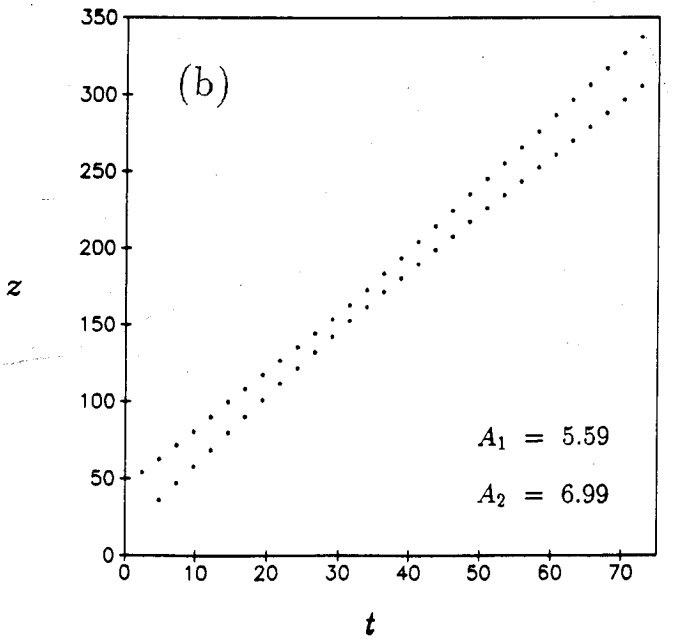

Figure 7 Phase diagrams of wave position vs. time showing the uniform speeds before and after collision. (a) Run 4. (b) Run 8.

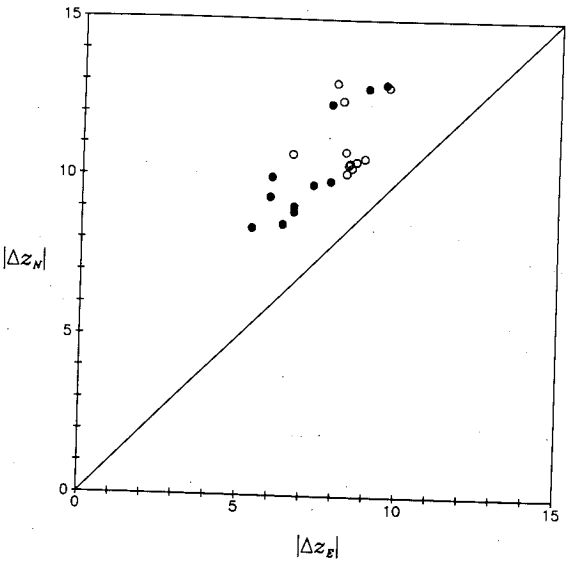

Figure 8 Numerically calculated phase jumps Δz_N vs. measured Δz_E phase jumps. ○, small waves; ●, large waves. The phase jumps of the small waves were all negative, but the absolute values are plotted.

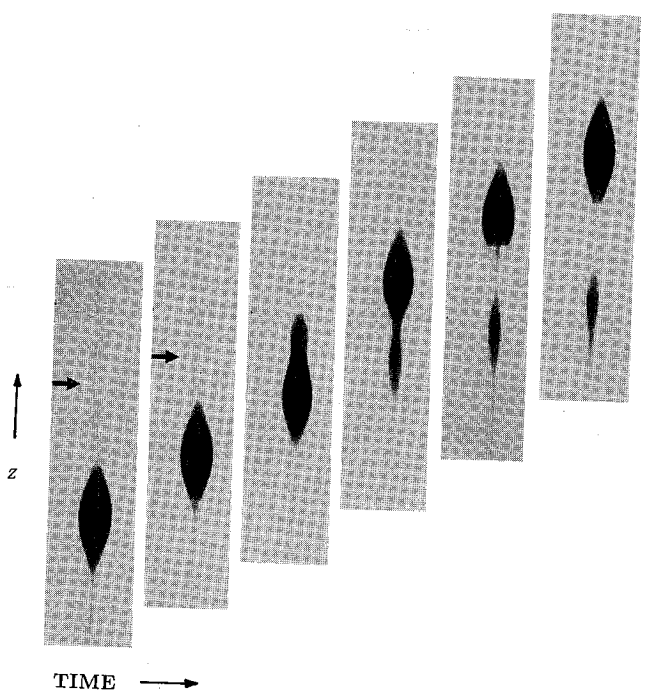

Figure 9 Sequence of photographs at equal time intervals showing the transfer of trapped fluid during wave interaction. The initially small lead wave and the conduit consist of undyed fluid and are not easily visible in the photographs. The arrows give the location of the lead wave in the first two frames. The trailing wave contains a parcel of dyed fluid.

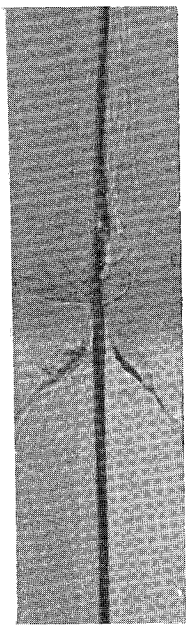

Figure 10 Shadowgraph showing a conduit penetrating the interface between two layers of external fluid. The upper layer is less dense and less viscous that the lower layer.

4.3 Layered External Fluids

Several preliminary experiments were performed to examine conduit and wave behavior in a vertically inhomogeneous external fluid. The experiments were conducted as described above except that a layer of 80:20 mixture by volume of Karo syrup to water was floated on a layer of pure Karo syrup. Figure 10 shows a shadow-graph of the interface and an established conduit. The viscous stress at the conduit walls is sufficient to cause an uplift of the interface and a secondary circulation in the upper layer. Heavy viscous fluid from the lower layer is dragged into the upper layer as a coating around the conduit. This may have implications for conduits in a layered mantle. Passage of solitary waves through the interface does not change these features. The waves are able to pass through the interface with no significant changes in properties. No wave fissioning, which can occur in inhomogeneous media (e.g., solitary surface waves over variable depth (Whitham, 1974)), was observed.

5. CONCLUSION

A conduit of buoyant low viscosity fluid rising through a more viscous fluid is another physical system in which solitary waves and soliton-like behavior are robust features. Individual wave characteristics of shape and phase speeds derived from experiments compared quite well with theoretical predictions. Larger amplitude waves tended to be predicted less well, presumably due to the presence of large wave slopes. Interactions of waves resulted in a measurable phase shift

without significant changes in individual wave charactersitics. Numerical calculations with the conduit equations overpredicted the magnitude of the phase shift.

The theoretical and experimental demonstration of mass trapping may have significant implications for transport in deep mantle plumes. In an examination of convective processes at the core–mantle boundary Olson *et al.*, (1987) conducted numerical simulations of two-dimensional convection in a fluid with a temperature dependent viscosity. A robust feature of their calculations was the development of vertical conduits and the unsteady generation of waves on the conduits. The waves propagated vertically away from the lower heated (core–mantle) boundary. As shown in Section 2 these waves contain trapped fluid which propagates with the wave. In contrast, the solitary wave solutions to the one-dimensional compaction driven flow equations do not contain trapped packets of melt which propagate with the wave (Scott and Stevenson, 1986). Fluid particles undergo a finite displacement upon passage of the wave as in the case of shallow water solitary waves.

This mass trapping property of conduit waves is important for two reasons. The first is that the wave velocity is faster than the maximum undisturbed conduit velocity, so that material packets will be delivered to the upper mantle more quickly than by regular conduit flow. Secondly, material transported with the waves will be mixed significantly less than material in a central streamline undergoing regular pipe flow (Whitehead and Helfrich, 1988). Newly injected material in regular pipe flow will be stretched by the shear and enhanced lateral diffusion will occur (Taylor, 1953). Injected material that forms solitary waves will be retained within the dividing streamline and thus remain isolated.

References

Barcilon, V. and Richter, F. M., "Nonlinear waves in compacting media," *J. Fluid Mech.* **164,** 429 (1986).

Batchelor, G. K., *An Introduction to Fluid Dynamics*, Cambridge University Press (1967).

Morgan, W. J., "Convective plumes in the lower mantle," *Nature* **230,** 42 (1971).

Olson, P. and Christensen, U., "Solitary wave propagation in a fluid conduit within a viscous matrix," *J. Geophys. Res.* **91(B),** 6367 (1986).

Olson, P., Schubert, G. and Anderson, C., "Plume formation in the D''-layer and the roughness of the core–mantle boundary," *Nature* **327,** 409 (1987).

Richter, F. M. and McKenzie, D. P., "Dynamical models for melt segregation from a deformable matrix," *J. Geol.* **92,** 729 (1984).

Scott, D. R. and Stevenson, D. J., "Magma solitons," *Geophys. Res. Lett.* **11,** 1161 (1986).

Scott, D. R. and Stevenson, D. J., "Magma ascent by porous flow," *J. Geophys. Res.* **91(B9),** 9283 (1986).

Scott, D. R., Stevenson, D. J. and Whitehead, J. A., "Observations of solitary waves in a viscously deformable pipe," *Nature* **319,** 759 (1986).

Taylor, G. I., "Dispersion of a soluble matter in solvent flowing slowly through a tube," *Proc. R. Soc.* **A256,** 186 (1953).

Whitehead, J. A., "A laboratory demonstration of solitons using a vertical watery conduit in syrup," *Am. J. Phys.* **55,** 998 (1987).

Whitehead, J. A. and Helfrich, K. R., "The Korteweg–de Vries equation from laboratory conduit and magma migration equations," *Geophys. Res. Lett.* **13,** 545 (1986).

Whitehead, J. A. and Helfrich, K. R., "Wave transport of deep mantle material," *Nature* **336,** 59 (1988).

Whitehead, J. A. and Luther, D. S., "Dynamics of laboratory diapir and plume models," *J. Geophys. Res.* **80,** 705 (1975).

Whitham, G. B., *Linear and Nonlinear Waves*, Wiley (1974).

GEOPHYSICAL AND ASTROPHYSICAL FLUID DYNAMICS

GENERAL INFORMATION

AIMS AND SCOPE

Geophysical and Astrophysical Fluid Dynamics exists for the publication of original research papers and short communications, occasional survey articles and conference reports on the fluid mechanics of the earth and planets, including oceans, atmospheres and interiors, and the fluid mechanics of the sun, stars and other astrophysical objects. In addition, their magnetohydrodynamic behaviors are investigated. Experimental, theoretical and numerical studies of rotating, stratified and convecting fluids of general interest to geophysicists and astrophysicists appear. Properly interpreted observational results are also published. Notes for contributors can be found at the back of the journal.

Subscription rates
Four issues per volume. Current Volume Block: 50–52
Orders may be placed with your usual supplier or directly with Gordon and Breach Science Publishers Inc., c/o STBS Ltd., P.O. Box 197, London WC2E 9PX. UK. Journal subscriptions are sold on a volume basis only; single issues are not available separately. Claims for nonreceipt of issues should be made within three months of publication of the issue or they will not be honored without charge. Subscriptions are available for microform editions. Details will be furnished upon request.

SUBSCRIBER INCENTIVE PLAN (SIP)
SIP offers a system of discounts to university libraries that maintain a continuous subscription to our journals. Prices to SIP members are at least 10% lower than the 1990 university price. For details on SIP and the range of benefits it offers, please write to STBS.

Distributed by STBS Ltd., P.O. Box 197, London WC2E 9PX, England, UK.
Printed in the United Kingdom by Bell and Bain Ltd., Glasgow.

MARCH 1990